© 2016

# REGULAR AND IRREGULAR DYNAMICS OF SPIN-POLARIZED WAVEPACKETS IN A MESOSCOPIC QUANTUM DOT AT THE EDGE OF TOPOLOGICAL INSULATOR

**D. V. Khomitsky**[*], **A. A. Chubanov**, **A. A. Konakov**

*Department of Physics, Lobachevsky National Research State University of Nizhni Novgorod*
*603950, Nizhni Novgorod, Russia*

The dynamics of Dirac–Weyl spin-polarized wavepackets driven by a periodic electric field is considered for the electrons in a mesoscopic quantum dot formed at the edge of the two-dimensional HgTe/CdTe topological insulator with Dirac–Weyl massless energy spectra, where the motion of carriers is less sensitive to disorder and impurity potentials. It is observed that the interplay of strongly coupled spin and charge degrees of freedom creates the regimes of irregular dynamics in both coordinate and spin channels. The border between the regular and irregular regimes determined by the strength and frequency of the driving field is found analytically within the quasiclassical approach by means of the Ince–Strutt diagram for the Mathieu equation, and is supported by full quantum mechanical simulations of the driven dynamics. The investigation of quasienergy spectrum by Floquet approach reveals the presence of non-Poissonian level statistics, which indicates the possibility of chaotic quantum dynamics and corresponds to the areas of parameters for irregular regimes within the quasiclassical approach. We find that the influence of weak disorder leads to partial suppression of the dynamical chaos. Our findings are of interest both for progress in the fundamental field of quantum chaotic dynamics and for further experimental and technological applications of spin-dependent phenomena in nanostructures based on topological insulators.

## 1. INTRODUCTION

Recently, the growing attention in various fields of fundamental science has started to focus on the properties of so-called Dirac–Weyl fermions [1]. We can mention just a few examples here in elementary particle physics, massless neutrinos are described as Weyl fermions [2]; in quantum optics, laser-induced excitations in the system of ultracold atoms in optical superlattices have such properties [3]; and, of course, numerous manifestations are known in condensed matter physics [4]. In solid-state systems, interestingly, Dirac–Weyl fermions can have different dimensionalities, such as 3D low-energy long-wavelength excitations in Weyl semimetals [5], well-known 2D electron and hole excitations near the Brillouin zone $K$ point in graphene [6] as well as on the surface of 3D topological insulators (TI) [7], and 1D Weyl fermions at the edge of graphene [8] or at the edge of 2D TI [7].

In this paper, we are interested in properties of the simplest 1D Dirac–Weyl fermions, which in the case of free particles can be described by the Hamiltonian

$$H_0 = \hbar v_F k_i \sigma_j, \qquad (1)$$

where the parameter $v_F$ is the electron velocity at the Fermi level, and $k_i$ and $\sigma_j$ are (generally different) components of the wavevector and the Pauli spin vector, both depending on the system geometry. The Pauli vector prescribes that the wave function is two-component, but its physical meaning depends on the realization of Weyl fermions, and it could represent spin, pseudospin or, generally speaking, some other "effective spin" degrees of freedom. Despite the simplicity of Hamiltonian (1), it maintains all general properties of the Dirac–Weyl fermions, namely, their linear dispersion and "two-bandedness". The 1D excitations described by Hamiltonian (1) can be most easily produced at the edge of a 2D topological insulator, and we therefore assume this special case for definiteness in what follows. These materials represent the condensed matter state with a bulk band gap and a propagating edge

or surface states that are protected from backscattering by time-reversal symmetry and have energies within the bulk gap. Thus, in a 2D TI, an efficient transport through 1D edge channels can be produced.

While static properties of Dirac–Weyl fermions at the edge of 2D TIs are well described [7], much less is known about evolution of the Dirac states under external driving fields. The dynamics of a quantum system can often be classified as one of two limit cases: the few-level dynamics and the evolution involving very many levels, usually referred to as quasiclassical dynamics. In the latter case, there are commonly used analogies between the quantum evolution and the corresponding dynamics of a classical counterpart. The problem with applying this approach to Dirac–Weyl fermions is that no direct classical counterpart is available. The same questions arise in investigating special regimes of dynamics called irregular, stochastic, or chaotic dynamics. It is still an open question which type of dynamics can be called quantum chaotic dynamics when a system lacks a direct classical counterpart. Several approaches to quantum stochasticity have been successfully developed over many years [9–11]. In a quantum system with a large number of energy levels $N \gg 1$, the quasiclassical approach can be applied regardless of whether the system has a classical counterpart. The general rule states that a classically chaotic systems also demonstrates certain chaotic dynamics in the quantum regime. However, it is not clear whether any quantum system without the classical counterpart such as Dirac–Weyl fermions would demonstrate stochastic behavior under particular circumstances. Several approaches aimed at establishing relations between quantum and classical systems with chaos have been proposed, including the studies of irregular dynamics in condensed matter systems [11] and quantum dots [12]. The relations between classical and quantum chaotic systems have been established in properties such as the structure of the quasienergy spectra and the phenomena of quantum diffusion in the Hilbert space. Here, the analogies between the diffusion along the resonance eigenstates and along the separatrices in the corresponding classical system have been found [10, 11], including an analogue of Arnol'd diffusion in quantum systems subject to periodic driving [13].

Among the simplest and important systems without a classical counterpart are low-dimensional structures where the spin is strongly coupled to the orbital degrees of freedom, including those with spin–orbit coupling (SOC) and surfaces of TIs. The importance of semiconductor structures with a strong SOC has been recognized during the last decade, and a significant progress can be observed in a corresponding field of nanophysics called spintronics [14,15]. We may expect a similar rich variety of the results for condensed matter systems with Dirac cones in the electron spectra as the field of topological insulators continues to grow [7].

The presence of SOC leads to correlation between space and spin degrees of freedom and, thus, creates a possibility of nontrivial dynamics or evolution in coupled coordinate and spin channels. It is known, for example, that the combined effects of SOC and the resonance in a multi-level system subject to strong driving can lead to unusual nonlinear behavior in well-known regimes such as the quasiclassical dynamics of the electron in a double quantum dot [16], or the Rabi frequency dependence on the driving strength in the electric dipole spin resonance in a double quantum dot [17]. It was also shown that in a double quantum dot with SOC, other interesting regimes can develop such as phase synchronization, or even chaotic spin-dependent dynamics [18]. Other examples can be found in a 2D mesoscopic semiconductor quantum dot with SOC [19], and in the 2D deformed harmonic oscillator potential with SOC [20]. In these studies, the non-Poissonian level statistics has been found, which indicates the presence of quantum chaos. In our recent paper [21], we have found the development of strongly irregular dynamics in this system under the periodic driving by an electric field, which manifested itself in both charge and spin channels. Such a nontrivial spin-dependent evolution of quantum states should also develop in the driven dynamics of electrons on the surface of 3D TIs and at the edge of 2D TIs, where the Dirac–Weyl Hamiltonian can be described as the limit case of the electron Hamiltonian with the extremely high linear-in-k SOC.

The major problem of establishing the quantum–classical correspondence in such spin-dependent systems is the mentioned absence of a direct classical counterpart, which creates obstructions to describing such systems in terms of the classical chaotic dynamics. Therefore, some techniques have to be found that allow distinguishing between regular and irregular dynamics in purely quantum system. The primary tools for overcoming such difficulties are the Floquet analysis for periodic driving [10, 11, 13] and the analysis of transport properties reflecting the regular or chaotic structure of the energy spectrum and eigenstates [12, 22].

In the Floquet analysis, one may look at the degree of delocalization of the Floquet eigenstates in the Hilbert space of basis states of a bounded quantum system or the quasienergy level statistics, clearly indicating the possibility of diffusion and chaos development

[10, 11], and at the direct Fourier analysis of the observables, or quantum mean values [9, 23]. Other tools include the analysis of Poincaré sections built in various pairs of coordinates for both coordinate and spin degrees of freedom, not necessarily the canonically conjugate ones [21, 23], or the tracking of the evolution for the variance for the number of energy levels involved in the dynamics. Here, the growth of this variance indicates the development of a chaotic regime, and the saturation points to the transition to a quasiregular mode with a finite number of levels participating in the evolution [13, 21].

In this paper, we address the complex driven dynamics of Dirac–Weyl wavepackets representing the electrons localized in mesoscopic structures formed at the edge of HgTe/CdTe 2D topological insulator by magnetic barriers. Such barriers are required due to the effect of Klein tunneling prohibiting the purely electrostatic confinement of the Dirac–Weyl fermions with Hamiltonian (1). Our general aim is to find whether the dynamics of a Dirac–Weyl wavepacket with Hamiltonian (1) in a quantum dot (QD) formed at the edge of the TI is regular or irregular, if the packet is driven by a monochromatic electric field. To find this, we consider the time evolution of various observables associated with the wavepacket dynamics, their Fourier spectra, and the "phase space" portraits of different pairs of variables, for both coordinate and spin degrees of freedom. We find that certain properties of driven evolution are sustained for wavepackets of different shape and are not smeared by a moderate disorder potential.

This paper is organized as following. In Sec. 2, we introduce a model of quantum states in a 1D QD at the edge of 2D TI based on the HgTe/CdTe quantum well in the case of magnetic barriers with finite transparency where the wavefunctions have nonvanishing tails inside the barriers. We consider the case of a macroscopic QD with a length $L = 3\ \mu$m in order to obtain a large number of levels ($N_{max} \approx 100$) in the TI bulk gap, which is desirable in order to capture the quasiclassical traits of chaos development. Such an assumption of a long 1D mesoscopic QD is feasible because the experiments report rather high values of mean free paths in such structures, reaching several microns [7]. In Sec. 3, we perform a quasiclassical analysis of the driven dynamics and find the correspondence between the equations for the spin dynamics and the Mathieu equation, and identify the associated instability boundaries indicating the possible onset of chaotic dynamics. In Sec. 4, we describe the Floquet eigenstates, which may indicate the diffusion in the Hilbert space showing the possibility of chaotic dynamics. In Sec. 5, we consider the evolu-

tion in the clean limit (no static disorder or noise) for the electron inside the QD, where the electron is represented via a spin-polarized wavepacket. In that Section, we consider the initial wavepacket described by a wide envelope function in the coordinate space and by a narrow distribution in the Hilbert space of eigenstates of the unperturbed Hamiltonian. Such a narrow distribution allows drawing the correspondence between the full quantum mechanical treatment in that section and the quasiclasical approach described in Sec. 3. We consider the evolution under a monochromatic driving electric field, and describe it in terms of phase-space plots generalized also to pairs of nonconjugate spin variables. We also analyze the Fourier spectra, diffusion in Hilbert and coordinate spaces, and the Lyapunov exponent. In Sec. 6, we add the random disorder potential representing the nonideal character of a real nanostructure as well as possible noise in the system and study the driven evolution there. In that section, we take a narrow initial wavepacket that has a wide distribution along the basis states of the unperturbed Hamiltonian, making only the full quantum mechanical treatment valid. We find that the qualitative features of the driven evolution are the same for both types of wavepackets considered here and in the preceding section, which provides additional justification for the quasiclassical treatment in Sec. 3. Finally, we present our conclusions in Sec. 7.

## 2. MODEL FOR QUANTUM STATES

One of the first examples of Dirac–Weyl fermions in condensed matter were the edge states in the HgTe/CdTe quantum wells, where the tuning of the well width may create the phase where topologically protected edge states exist [7, 24]. It is known, however, that the applications of TI in nanoelectronic devices require the fabrication of localized small-to-medium size object like quantum dots. Several models of QD formation at the edge of a TI have been proposed during the last years [25, 26]. Most of them relevant to 1D QDs at the edge of a 2D TI deal with simplified assumptions of nontransparent magnetic barriers, which are required to confine the electrons with a massless Dirac–Weyl spectrum [7]. It should be mentioned that similar methods of confinement by creating a gap in the spectrum by the magnetic field or other mass terms have also been proposed for other materials with Dirac–Weyl spectra such as graphene [27]. Under such assumptions, the spectrum of discrete energy levels inside a QD forms a set of equidistant levels located in two ladders above and below the Dirac point of the TI, where two linear

dispersion branches cross [25]. For each level, the corresponding eigenstate is a two-component spinor with a certain spin polarization, which makes this system a promising candidate for studying a driven dynamics excited by the external electric field tuned to match the interlevel resonance splitting.

In this paper, we use the envelope function approximation with the effective Hamiltonian for the 1D electron in a QD confining the propagating spin-polarized states at the edge of the 2D HgTe/CdTe TI:

$$
\begin{aligned}
H_{QD} = \\
= \hbar v_F k_y \sigma_z - M_0 \theta(-y)\left(\sigma_x \cos\theta_0 + \sigma_y \sin\theta_0\right) - \\
- M_L \theta(y-L)\left(\sigma_x \cos\theta_L + \sigma_y \sin\theta_L\right).
\end{aligned} \tag{2}
$$

Here, the first term is the effective Dirac–Weyl Hamiltonian (1) for unperturbed gapless edge states on the boundaries of the TI. The Fermi velocity $v_F$ is determined by the HgTe layer thickness, and in our model we take the value $v_F = 5.3 \cdot 10^7$ cm/s and consider the band gap in HgTe/CdTe to be around 40 meV in the inverted regime, which corresponds to the quantum well width in the range 8–9 nm [7]. The second and third terms in (2) describe the local exchange interaction between the electron near the edge of the quantum well and the magnetization of magnetic stripes. The magnetization of both contacts is assumed to be uniform without any domain structure. This situation is typical for nanomagnets with a size less than 100 nm in at least one direction [28]. The barrier magnitudes $M_0$ and $M_L$ can be viewed as exchange energies. Both magnetic contacts are located along the TI edge at $y = 0$ and $y = L$, forming a 1D QD with the width $L$, as is shown schematically in Fig. 1a. The QD length $L = 3$ μm in our model is sufficiently large to justify the application of the envelope function approximation. We consider the barriers with finite transparency by choosing finite amplitudes $M_0$ and $M_L$, which are taken as to cover the whole band gap of the HgTe/CdTe quantum well. The size of the magnets along the TI edge is considered to be comparable with the QD size, and we can therefore assume them to be infinite in this direction, because the wavefunction of the QD states decays exponentially into barriers on the scale that is much smaller than the magnet length, as we see below. The angles $\theta_0$ and $\theta_L$ describe the orientation of the magnetization in the respective left and right barriers. Our Hamiltonian is the generalization of the previously derived model for a QD with impenetrable barriers [25] to the more realistic case of the barriers with finite transparency, reflected in their finite height $M_{0,L}$. We note that the few-electron regimes are usually desirable for operations of QDs as a

qubit or other information processing devices. Hence, we believe that it is necessary to use dielectric magnetic materials in order to prevent the excessive leak of electrons from the leads into the QD.

The stationary 1D Schrödinger equation $H_{QD}\Psi = E\Psi$ for the two-component envelope function $\Psi = (\psi_1(y), \psi_2(y))$ is augmented by the boundary conditions at $y = 0$ and $y = L$ that can be derived from its integration over an infinitesimal small region near the boundary, yielding the requirements

$$
\begin{aligned}
\Psi(-0) = \Psi(+0), \\
\Psi(L-0) = \Psi(L+0),
\end{aligned} \tag{3}
$$

which mean that the envelope function must be continuous at the boundaries between the QD and the barriers. The spatial dependence of the solution for a confined state with an energy $E < (M_0, M_L)$ inside the barriers at $y < 0$ and $y > L$ has the form of decaying underbarrier exponentials,

$$
\Psi_{y<0} = B \begin{bmatrix} 1 \\ -\dfrac{i\sqrt{M_0^2 - E^2} + E}{M_0} e^{i\theta_0} \end{bmatrix} \times \\
\times \exp\left(\frac{\sqrt{M_0^2 - E^2}}{\hbar v_F} y\right), \quad (4)
$$

$$
\Psi_{y>L} = D \begin{bmatrix} 1 \\ \dfrac{i\sqrt{M_L^2 - E^2} - E}{M_L} e^{i\theta_L} \end{bmatrix} \times \\
\times \exp\left(-\frac{\sqrt{M_L^2 - E^2}}{\hbar v_F} y\right), \quad (5)
$$
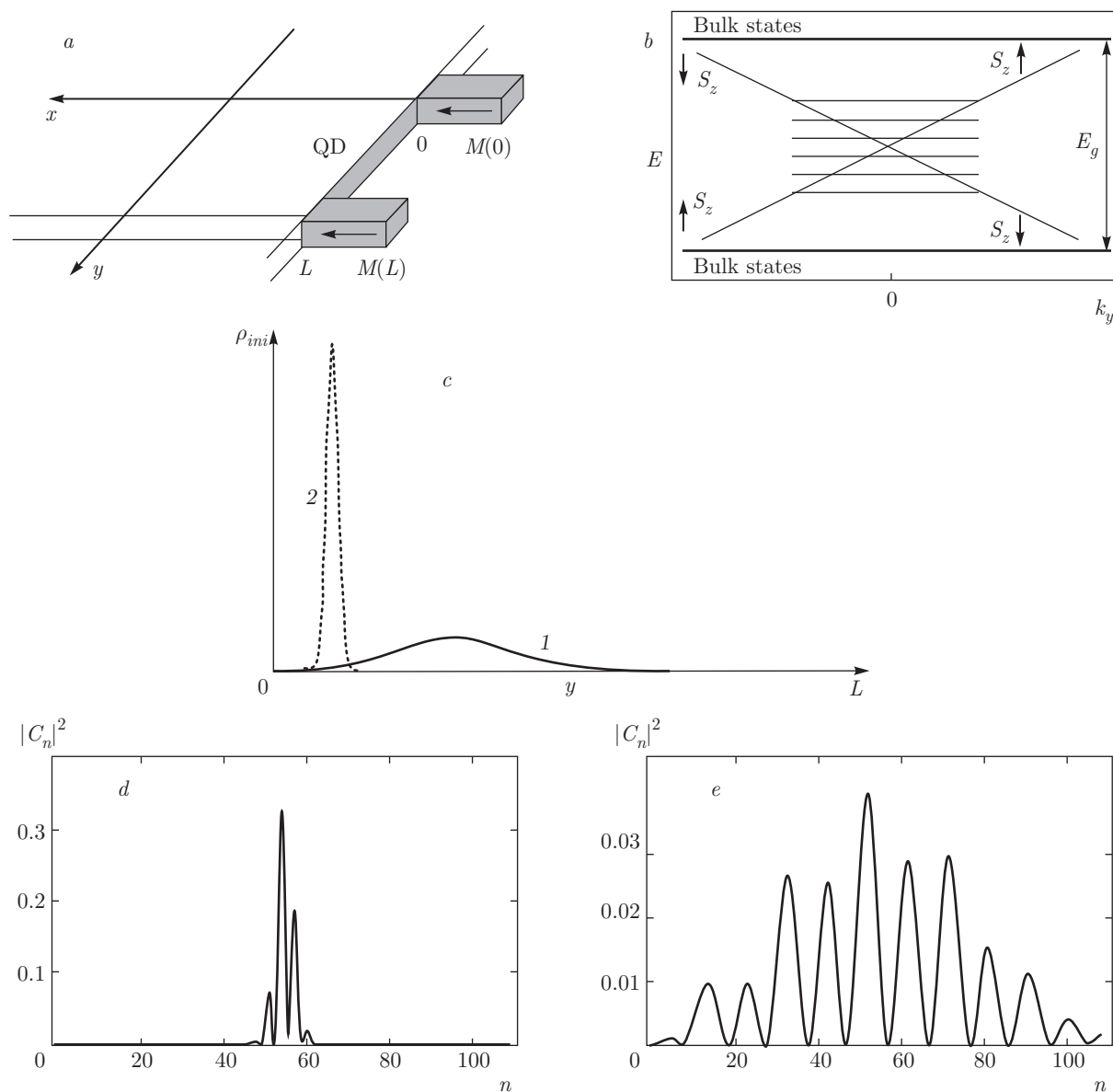
and the eigenstate inside the QD is a spinor with a real wavenumber in its exponents,

$$
\Psi_{QD} = \begin{bmatrix} C_1 e^{iEy/\hbar v_F} \\ C_2 e^{-iEy/\hbar v_F} \end{bmatrix}, \tag{6}
$$

where the coefficients $B$, $C_1$, $C_2$, and $D$ are determined from boundary conditions (3), and the energy $E$ is found from the corresponding secular equation with Hamiltonian (2). We note that states (4)–(6) correspond to the spin polarization that is always in the plane of the 2D TI, that is, $S_z = 0$.

System of equation (3) for envelope function (4)–(6) can be solved analytically for nontransparent barriers, where the wavefunction does not enter the underbarrier region [25, 26] and a sequence of up and down strictly equidistant energy levels

$$
E_{n_0}^{(0)} = \Delta E^{(0)} \left(n_0 + \frac{1}{2} + \frac{\theta_L - \theta_0}{2\pi}\right) \tag{7}
$$

**Fig. 1.** (*a*) Schematic view of a 1D QD (gray strip) with length $L$ formed by two magnetic barriers $M_0$ and $M_L$ at the edge of 2D topological insulator in a HgTe/CdTe quantum well. The dot length is $L = 3$ $\mu$m, the barrier height is $M_0 = M_L = E_g/2$, where $E_g = 40$ meV is the band gap for the host material observed for typical HgTe/CdTe quantum well samples, and the arrows inside the barriers represent their polarizations actually considered in our model. (*b*) Schematic representation of the discrete energy levels inside the QD with the interlevel distance shown as a guide to the eye and not to scale. The linear dispersion branches are shown for the free Weyl Hamiltonian (1) describing edge states, with the corresponding spin mean values $S_z$. The boundaries of the bulk energy gap $E_g$ are plotted above and below as horizontal lines. (*c*) Probability density distribution for Gaussian spin-polarized wavepackets with different widths and center locations representing the initial condition for the dynamics of the electron injected into the QD shown for wide (solid line *1*) and narrow (dashed line *2*) wavepackets. (*d*),(*e*) Distribution of the expansion coefficients $|C_n|^2$ of the initial states from panel (*c*) in the space of basis states for (*d*) the wide initial packet (1) and (*e*) the narrow initial packet (2)

($n_0 = \pm 1, \pm 2, \dots$) is formed with a spacing that is independent of $\theta_L - \theta_0$,

$$\Delta E^{(0)} = \frac{\pi \hbar v_F}{L}. \qquad (8)$$

In this paper, we consider the case of parallel orientation $\theta_0 = \theta_L = 0$ because it follows from (7) and (8) that different angles of magnetization inside the barriers mostly define the internal structure of corresponding eigenstates and their spin polarization inside the QD, and do not affect the level spacing in the idealized case of nontransparent barriers, which determines the primary frequency of the driving field in our model. This result maintains in the case of transparent magnetic barriers considered in our model (2). One may expect that the variable difference between $\theta_0$ and $\theta_L$ would lead to the formation of quantum states with a different spatial symmetry, but in our dynamical problem this would produce only quantitative effects on the structure of matrix elements of the external perturbation, and thus only minor effects on the dynamical properties that are in the focus of our study. Besides, we choose equal amplitudes of magnetic barriers $M_0 = M_L$, which creates a QD with a symmetric potential profile, although various combinations of $M_0$, $M_L$, $\theta_0$, and $\theta_L$ can be equally considered if other materials and/or experimental setups are chosen.

In our model, the spectrum cannot be found analytically, and has to be obtained from a transcendental equation, which leads in general to a nonequidistant spectrum with a nonuniform level spacing $\Delta E$. However, for a mesoscopic QD with $L = 3$ $\mu$m, it follows from (8) that $\Delta E^{(0)} \approx 0.38$ meV and the condition $\Delta E^{(0)} \ll M_{0,L}$ is satisfied, meaning that there are many levels below the barriers ($N_{max} \approx 100$), the level spacing $\Delta E$ is very close to the equidistant value $\Delta E^{(0)}$ in (8).

The scheme of the discrete energy levels inside the QD is presented in Fig. 1$b$ with a large interlevel distance, which is shown as a guide to the eye and not to scale. Together with the discrete levels, we plot the linear dispersion branches of Weyl Hamiltonian (1) describing the edge states [7] before the confining barriers are applied, together with corresponding $z$-aligned mean spin values $S_z$ and the boundaries of the bulk energy gap $E_g = 40$ meV. This gap allows restricting the barrier width by $M_0 = M_L = E_g/2$, because only the edge states within the bulk gap are relevant for the edge QD, where they are not masked by the bulk states.

Our final task considering the model of quantum states inside the QD is the choice of the localized initial condition for the dynamical problem representing a spin-polarized electron that has been injected through one of the magnetic barriers into the dot. We model such a condition by a Gaussian wavepacket with two different widths and center locations, with their probability density distribution shown in Fig. 1$c$ by the solid and dashed lines. In terms of the spatial size, the respective packets widths are 1 and 0.1 microns, which are reasonable values for the semiconductor structures being considered, where the mean free path for the electron is about 3 microns [7]. We refer to these packets as wide and narrow throughout the text, and assume the zero mean value of the initial quasimomentum $\overline{k_y}(0) = 0$. The spin polarization for the corresponding spinor representing the initial packet is chosen to coincide with the magnetization of the magnetic barrier (or electrode) from which the packet has been injected, that is, the $S_x = 1$ polarization of the left barrier, because the majority of the electrons traveling through a magnetic materials without special tuning usually gain the polarization from the host material. The initial condition $\Psi_0(y)$ has to be decomposed over the basis states $\Psi_n(y)$ inside the QD for further treatment of its evolution, that is, the coefficients $C_n$ in the decomposition $\Psi_0 = \sum_n C_n \Psi_n(y)$ have to be found by standard methods. The structure of their absolute value distribution $|C_n|^2$ in the space of basis states is shown in Fig. 1$d$ and $e$ for two initial packets from Fig. 1$c$. As expected, the wider packet in real space is described by a narrow distribution of $|C_n|^2$ in the Hilbert space compared to the narrow packet. We consider the driven dynamics for both types of wavepackets in the next sections, and we see that the difference in their shape in the coordinate or Hilbert spaces leaves certain dynamical features qualitatively the same, which allows considering our finding as relevant for various types of initial conditions.

## 3. QUASICLASSICAL DYNAMICS

We start with the application of the quasiclassical approach to the driven dynamics for the Hamiltonian

$$H = H_{QD} + V(y,t), \qquad (9)$$

where $H_{QD}$ is stationary Hamiltonian (2) and $V(y,t)$ is the driving term describing the electric field inside the QD at $0 < y < L$,

$$V(y,t) = e\mathcal{E}_0 y \cos \omega_0 t, \qquad (10)$$

where $e$ is the elementary charge, $\omega_0$ is the driving frequency, and $\mathcal{E}_0$ is the electric field strength. It corresponds to the spatially uniform and harmonic electric

field directed along the TI edge. This field can be generated by additional electrostatic gates arranged close to the bounding magnetic barriers. We consider the quasistationary field that is produced by the modulation of the gate potential and assumed to be spatially uniform on the QD scale $L = 3\ \mu$m.

The mesoscopic size of our QD ($3\ \mu$m) and the large number of energy levels (about 100) allows the application of the quasiclassical approach. This approach can be applied for systems with and without a direct classical counterpart, including the ones with spin-orbit coupling in nanostructures if their dimensions generate a quasiclassically high number of energy levels [16]. In the framework of this approach, we consider only the evolution of quantum mechanical mean values. The evolution of the mean value $\overline{x}(t)$ corresponding to a time-independent operator $x$ is governed by the equation

$$\frac{d\overline{x}(t)}{dt} = \frac{i}{\hbar}\overline{[H, x]}, \qquad (11)$$

where $\overline{(\ldots)}$ stands for the quantum mechanical averaging in a given state $\Psi(\mathbf{r}, t)$. By applying Eq. (11) to the dynamics of the average of the operator product $\overline{AB}$, we can treat it as a product of two averages $\overline{A} \cdot \overline{B}$ if the distribution of the coefficients $C_n$ for the wavefunction decomposition over the basis states $\phi_n$ is a narrow function centered at certain $\overline{n} \gg 1$. This means that the width $\delta n$ satisfies the condition $\delta n \ll \overline{n}$, although being quasiclassically large, $\delta n \gg 1$, as is assumed in the quasiclassical approach used in this section. Our full quantum mechanical simulations presented in the next sections support this approximation for the parameters of the evolution. In particular, in Sec. 5 we perform the full quantum mechanical simulation for the wavepacket that is initially described by a narrow distribution in the Hilbert space and satisfies the criteria for the quasiclassical treatment mentioned above. By contrast, in Sec. 6 we take an initially wide packet in the Hilbert space, for which only the full quantum mechanical simulation is applicable. We see in what follows that the qualitative results for the evolution are largely the same in both cases, which is a strong evidence of a correspondence between the quasiclassical and full quantum approaches presented in this paper.

For Hamiltonian (9) with the parallel orientation of the magnetic barriers $\theta_0 = \theta_L = 0$, we use (11) to obtain the following set of equations for the evolution of the coordinate and spin mean values inside the QD:

$$\frac{d\overline{y}(t)}{dt} = v_F\overline{\sigma_z}(t), \qquad (12a)$$

$$\frac{d\overline{k_y}(t)}{dt} = \frac{\omega_b}{2}\frac{\partial F_b}{\partial y}\overline{\sigma_x}(t) - \frac{e\mathcal{E}_0}{\hbar}\cos\omega_0 t, \qquad (12b)$$

$$\frac{d\overline{\sigma_x}(t)}{dt} = -2v_F\overline{k_y}(t)\overline{\sigma_y}(t), \qquad (12c)$$

$$\frac{d\overline{\sigma_y}(t)}{dt} = 2v_F\overline{k_y}(t)\overline{\sigma_x}(t) + \omega_b F_b(y)\overline{\sigma_z}(t), \qquad (12d)$$

$$\frac{d\overline{\sigma_z}(t)}{dt} = -\omega_b F_b(y)\overline{\sigma_y}(t). \qquad (12e)$$

The frequency $\omega_b = 2M_0/\hbar$ and the function $F_b(y) = \Theta(-y) + \Theta(y - L)$ are associated with the presence of magnetic barriers. Although the function $F_b(y)$ is nonzero only in the barrier regions $y < 0$ and $y > L$, while we study the quasiclassical dynamics within the QD for $0 < y < L$, we need to keep it at least in Eq. (12e) because it determines the evolution of the $\sigma_z$ spin component. This means that the coupling to the magnetic barriers is essential for the driven dynamics to be initiated, which is confirmed by the full quantum mechanical calculations in the next sections.

System (12a)–(12e) is a system of differential equations with nonstationary coefficients, and cannot be solved analytically in the general case. This is a typical situation: for example, in [16], we mostly performed a computational analysis for a similar problem. But for some regimes of driving, certain analytic results can be obtained. For example, the harmonic time dependence of driving term (10) allows integrating Eq. (12b) directly inside the QD region $0 < y < L$ where $F_b \equiv 0$, yielding

$$\overline{k_y}(t) = \overline{k_{y0}} - \frac{e\mathcal{E}_0}{\hbar\omega_0}\sin\omega_0 t. \qquad (13)$$

Having determined the time dependence $\overline{k_y}(t)$, we can see that the other equations (12a), (12c)–(12e) are linear equations with periodic coefficients with respect to the time variable. It is known that such equations can demonstrate unstable solutions which, is often referred to as parametric resonance. Because all of the coordinate and spin variables are coupled through the equations in the system, it suffices to determine the boundary of that instability for at least one variable. If a variable demonstrates an irregular time dependence, the other coupled variables would also acquire similar behavior with time. The simplest analytic result leading to a well-known type of equation with instabilities can be obtained for the spin variable $\overline{\sigma_x}(t)$. By differentiating the left- and right-hand sides of (12c), we obtain the second-order equation

$$\frac{d^2\overline{\sigma_x}}{dt^2} + 2v_F\overline{k_y}\frac{d\overline{\sigma_y}}{dt} + 2v_F\frac{d\overline{k_y}}{dt}\overline{\sigma_y} = 0. \qquad (14)$$

We substitute the right-hand side of (12d) for the time derivative of $\overline{\sigma_y}$ in (14). We neglect the term with $F_b(y)$ for the quasiclassical treatment of the motion inside the dot because it is present only in the barrier regions. We then substitute the time dependence for $\overline{k_y}(t)$ from (13) in (14), and by using (12d), we replace $\overline{\sigma_y}$ with $(d\overline{\sigma_x}(t)/dt)/(-2v_F\overline{k_y}(t))$. As a result, we arrive at the equation for the $\overline{\sigma_x}$ alone:

$$\frac{d^2\overline{\sigma_x}}{dt^2} + f(t)\frac{d\overline{\sigma_x}}{dt} + g(t)\overline{\sigma_x} = 0, \tag{15}$$

where

$$f(t) = -\frac{1}{\overline{k_y}(t)}\frac{d\overline{k_y}(t)}{dt}, \quad g(t) = 4v_F^2\overline{k_y}(t)^2. \tag{16}$$

The first derivative of $\overline{\sigma_x}$ in (15) can be eliminated by introducing the new variable $\sigma_1(t)$ as

$$\overline{\sigma_x} = \sqrt{\overline{k_y}(t)}\sigma_1(t). \tag{17}$$

It is essential to note that our analysis in this section holds in the region $\overline{k_y}(t) > 0$, which means by checking (13) that a moderate electric field is allowed that does not lead to negative values of $\overline{k_y}(t)$ starting from a quasiclassically high initial value of $\overline{k_{y0}}$. We then introduce the dimensionless initial momentum as

$$k_0 = \frac{\overline{k_{y0}}\pi\hbar v_F}{e\mathcal{E}_0 L}, \tag{18}$$

and also define the electric-field-dependent frequency

$$\Omega = \frac{2v_F e\mathcal{E}_0}{\hbar\omega_0}. \tag{19}$$

We note that due to the condition $\overline{k_y}(t) > 0$ and expression (13), our analysis is restricted to the area where $k_0 > 1$, which, according to (18), means that we must stay within the quasiclassical region of a moderate electric field. Taking Eqs. (17), (18), and (19) into account and introducing the dimensionless time variable $\tau$ as

$$\omega_0 t = \tau, \tag{20}$$

we transform Eq. (15) to a second-order differential equation for $\sigma_1(\tau)$,

$$\frac{d^2\sigma_1}{d\tau^2} + \Theta(\tau)\sigma_1 = 0, \tag{21}$$

where

$$\Theta(\tau) = \frac{\Omega^2}{\omega_0^2}(k_0 - \sin\tau)^2 +$$
$$+ \frac{1}{2}\left[\frac{\sin\tau}{k_0 - \sin\tau} - \frac{3}{2}\frac{\cos^2\tau}{(k_0 - \sin\tau)^2}\right]. \tag{22}$$

Equation (21) is known as the Hill equation for a parametrically driven system, and the function $\Theta(\tau)$ is called the excitation function. It is known [29] that the Hill equation can demonstrate nonstationary behavior known as the parametric resonance. The specific form of the instability regions in the parameters space can be found either from the numerical analysis of the Hill equation, which implies solving it on a single period of the excitation function, or by the analytic approximation when the Hill equation is transformed into some other form with known areas of instability. The possibility of such a transformation crucially depends on the Fourier spectrum of the excitation function $\Theta(\tau)$. Our analysis of the Fourier components of function (22) has shown that it is the zeroth cosine harmonic and the first sine harmonic that dominate over the major part of our parameters, which include weak and moderate fields. We can expect that the effects of higher harmonics appearing in the cases where their amplitude increases tend to enlarge the instability regions found for the dominating lower harmonics. As regards the case where $k_0 \to 0$ in (22), it can be shown that we arrive at the excitation function where a single harmonic with the double frequency $2\omega_0$ dominates, and the subsequent analysis is similar to the case presented below with the substitution $\omega_0 \to 2\omega_0$. Hence, for the prediction of the instability effects, the Hill equation can be approximated by the equation where $\Theta(\tau)$ is replaced with a combination of its zeroth cosine and first sine harmonics. By making the phase shift $\tau \to \tau - \pi/2$, which changes $\sin\tau$ to $-\cos\tau$, we arrive at the following equation for $\sigma_1(\tau)$:

$$\frac{d^2\sigma_1}{d\tau^2} + (\delta + \varepsilon\cos\tau)\sigma_1 = 0. \tag{23}$$

Equation (23) is the Mathieu equation. This equation describes parametric resonance and has well-defined areas of stability and instability known as the Ince–Strutt diagram [29] in the plane of the parameters $(\delta, \varepsilon)$. The expressions for these parameters follow directly from the Fourier decomposition of the excitation function $\Theta(\tau)$:

$$\delta = \left(k_0^2 + \frac{1}{2}\right)\frac{\Omega^2}{\omega_0^2} + \frac{1}{4}\left(1 - \frac{k_0}{\sqrt{k_0^2 - 1}}\right), \tag{24}$$

$$\varepsilon = 2k_0\frac{\Omega^2}{\omega_0^2} + 2k_0\left(\frac{k_0}{\sqrt{k_0^2 - 1}} - 1\right) - \frac{3}{2\sqrt{k_0^2 - 1}}. \tag{25}$$

The parameters $(\delta, \varepsilon)$ defined in (24) and (25) in terms of the values of $\mathcal{E}_0$ and $\overline{k_{y0}}$ determine the regimes of parametric oscillations. The parameter $\delta$ approaches

a constant nonzero value when the electric field amplitude $\mathcal{E}_0 \rightarrow 0$, and this value is determined by the initial value of $\overline{k_{y0}}$. For moderate fields, the driving amplitude $\varepsilon$ behaves almost linearly with $\mathcal{E}_0$, as follows from definitions (18) and (19). According to the Ince–Strutt diagram, the onset of instability with increasing $\varepsilon$ is possible as the parametric resonance, which corresponds to the development of irregular dynamics for the mean of the spin variable $\overline{\sigma_x}$, and hence for the other coupled degrees of freedom in our system.

For our set of parameters (18) and (19), we can easily verify that for the driving frequency $\omega_0 = 0.58 \times$ $\times 10^{12}$ s$^{-1}$ considered below, the amplitude of the driving field as low as $\mathcal{E}_0 \approx 1$ V/cm can put our system into an instability area in the Ince–Strutt diagram. When this or higher electric field is driving the dynamics, we may expect the development of irregular regimes of spin and coordinate dynamics, which are coupled via system (12a)–(12e). In the next sections, we justify this finding by the fully quantum mechanical approach and a computational analysis for several values of the driving field.

## 4. QUANTUM DYNAMICS AND FLOQUET STATES

In this and in the next sections, we perform the quantum mechanical treatment of the electron state evolution under a spatially uniform and time-periodic electric field described by the term (10) in Hamiltonian (9). We intend to see the resonance dynamics, and hence the driving field frequency $\omega_0$ matches the level splitting $(E_{n_0+1} - E_{n_0})/\hbar$ in the region of most populated levels by the initial wavepacket, which is the middle part of the spectrum $n_0 \approx 54$ (see Fig. 1*d,e*). As we discussed in Sec. 2, in the case of a multi-level mesoscopic QD with the length $L = 3$ $\mu$m, the level splitting in the middle part of the spectrum is almost equidistant with the level spacing given by (8). This level splitting corresponds to the frequency $\omega_0 = 0.58 \cdot 10^{12}$ s$^{-1}$ being in the subterahertz range (the so-called W-band), for which we can consider the field as quasistationary, because $\hbar\omega_0$ is lower than the band gap by at least one order of magnitude. In this case, the scalar potential $V(y,t)$ is described by a small overall amplitude on the scale of the mesoscopic QD, and we can therefore introduce this potential into the envelope function Hamiltonian $H(y,t) = H_{QD} + V(y,t)$.

The periodic driving allows us to apply some of the tools from the Floquet analysis [10,11,13,17,21] in order to understand the system evolution. The most relevant

for our system is the structure of the Floquet states where the $s$th eigenstate is written as a vector $A_n^{(s)}$ in the Hilbert space of the basis states $\Psi_n(y)$. These vectors are the eigenvectors of the one-period propagator matrix $\mathbf{U}(T_0)$, where $T_0 = 2\pi/\omega_0$, which can be constructed from the evolution of the state $\Psi(y,t)$ in the basis of states $\Psi_n(y)$,
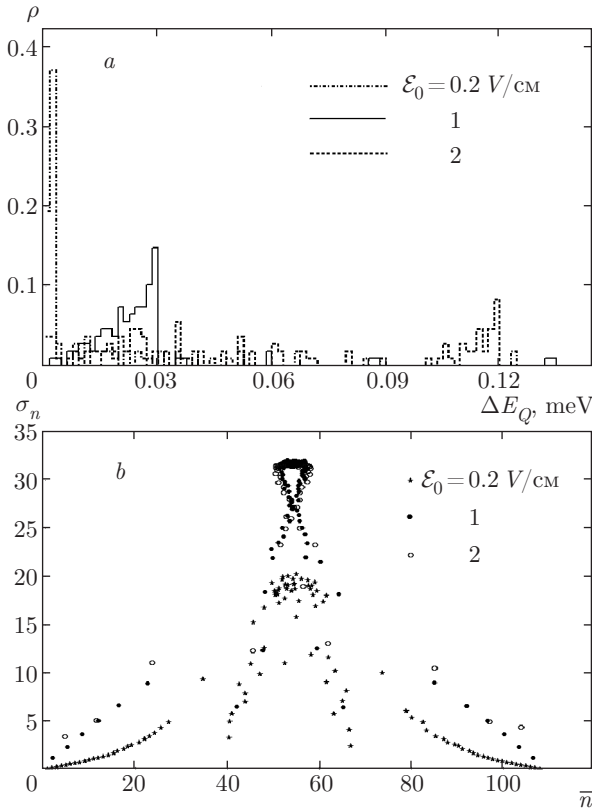
$$\Psi(y,t) = \sum_n C_n(t)\Psi_n(y), \qquad (26)$$

obeying the nonstationary Schrödinger equation for the envelope function

$$i\hbar\frac{\partial\Psi}{\partial t} = (H_{QD} + V(y,t))\Psi \qquad (27)$$

with the initial condition $C_n(0) = \delta_{nn_0}$ considered for all levels $n_0$ [10,13]. Equation (27) can be transformed into a system of ordinary linear differential equations for the coefficients $C_n(t)$ by projecting it on the basis of the states $\Psi_n(y)$, and this system is solved by standard numerical packages. The eigenvalues of $\mathbf{U}(T_0)$ labeled by the index $(s)$ have the form $\exp(-iE_Q^{(s)}T_0/\hbar)$, where $E_Q^{(s)}$ are the corresponding quasienergies. It is known that the information contained in the quasienergy level spacing distribution can describe both regular and chaotic regimes of the driven evolution, depending on whether such a distribution demonstrates the Poissonian or non-Poissonian behavior [10,11]. In Fig. 2*a*, we show the level spacing distribution $\rho(\Delta E_Q)$ for three different driving strengths in (10): $\mathcal{E}_0 = 0.2$ V/cm (dash-dotted curve), $\mathcal{E}_0 = 1$ V/cm (solid curve), and $\mathcal{E}_0 = 2$ V/cm (dotted curve). Although the number of energy levels in our system is too small to see a fully developed smooth distribution, it can be seen that for the weak driving, the level statistics looks like Poissonian one with most of the quasienergy levels grouped with a small spacing $\Delta E_Q$ of the order of 0.005 meV. As the driving increases, the level statistics progressively transforms into a non-Poissonian type with the maximum located near 0.03 meV for $\mathcal{E}_0 = 1$ V/cm and near 0.1 meV for $\mathcal{E}_0 = 2$ V/cm. According to the basic concepts of quantum chaos [10,11], this result can be viewed as an indication of the transition to chaos in our system as the periodic driving amplitude increases.

It is useful to compare the properties of the quasienergy level statistics with the results for the quasiclassical dynamics obtained in the preceding section. For the weak driving amplitude $\mathcal{E}_0 = 0.2$ V/cm, we have the following set of parameters (24) and (25) for the Mathieu equation by considering the conservative estimate of $\overline{k_{y0}} = \pi/L$: $\delta = 3.92$ and $\varepsilon = 0.2$. According to the Ince–Strutt diagram [29], this corresponds to

**Fig. 2.** (*a*) Level spacing distribution $\rho(\Delta E_Q)$ for the quasienergy levels for three different driving strengths $\mathcal{E}_0 = 0.2$ V/cm (dash-dotted curve), $\mathcal{E}_0 = 1$ V/cm (solid curve), and $\mathcal{E}_0 = 2$ V/cm (dotted curve). For the weak driving $\mathcal{E}_0 = 0.2$ V/cm, the level statistics is of the Poissonian type, which corresponds to the parameter area of the stable dynamics for Mathieu equation (23) obtained within the quasiclassical approach. For the stronger driving $\mathcal{E}_0 = 1$ V/cm and $\mathcal{E}_0 = 2$ V/cm, the level statistics transforms to a non-Poissonian type indicating the irregular regime of quantum dynamics, which corresponds to the unstable region of the quasiclassical approach. (*b*) Distribution of the Floquet quasienergy eigenstates in the $(\bar{n}, \sigma_n)$ coordinates, where $\bar{n}$ is the mean level number measuring the center of the Floquet state in the basis and $\sigma_n$ is the variance (width) in the Hilbert space, for driving strengths $\mathcal{E}_0 = 0.2$ V/cm (stars), $\mathcal{E}_0 = 1$ V/cm (filled circles), and $\mathcal{E}_0 = 2$ V/cm (open circles). The level variance $\sigma_n$ in general increases with the driving strength, and the extended states with $\sigma_n \approx 32$ exist at moderate and strong driving, meaning the presence of the diffusion in the Hilbert space into a substantial part of the spectrum and reflecting the possibility of irregular, or chaotic dynamics

the stability region, which is reflected in the Poissonian type of statistics in Fig. 2*a*, being a signature of regular dynamics. Then, as the electric field amplitude increases, we have $\delta = 4.08$ and $\varepsilon = 0.9$ for $\mathcal{E}_0 = 1$ V/cm, and $\delta = 4.4$ and $\varepsilon = 2.15$ for $\mathcal{E}_0 = 2$ V/cm. Both these

points in the $(\delta, \varepsilon)$ plane fall within the instability areas on the Ince–Strutt diagram, which means that the irregular dynamics is possible in the quasiclassical limit. These findings are justified by the full quantum mechanical treatment within the Floquet approach, being manifested in the transformation of the level statistics in Fig. 2*a* from the Poissonian to non-Poissonian type during the increase of the electric field amplitude.

Besides the quasienergy spectra, the structure of the Floquet eigenvectors $A_n^{(s)}$ can give much information regarding the possibilities of chaotic regimes for the evolution under periodic driving [10, 11, 13]. In particular, the presence of states which are extended in the Hilbert space formed by basis functions, that is, described by high values of the variance $\sigma_n$,

$$\sigma_n^2 = \sum_n (n - \bar{n})^2 |A_n|^2, \qquad (28)$$

where $\bar{n} = \sum_n n |A_n|^2$, corresponds to the regimes of diffusion in the Hilbert space of the initial state along such extended Floquet states, which can be viewed as a quantum counterpart of the classical chaos development. Hence, it is of interest to look at the distribution for all of the quasienergy eigenstates in the $(\bar{n}, \sigma_n)$ coordinates, where $\bar{n}$ is the mean level number measuring the center of the Floquet state in the basis and $\sigma_n$ is the variance, or width in the Hilbert space. In Fig. 2*b*, we plot the $(\bar{n}, \sigma_n)$ distributions for the Floquet eigenstates for three different driving strengths: $\mathcal{E}_0 = 0.2$ V/cm (stars), $\mathcal{E}_0 = 1$ V/cm (filled circles), and $\mathcal{E}_0 = 2$ V/cm (open circles). It is clear that the level variance $\sigma_n$ in general increases with the driving strength, which is the expected effect (although a certain saturation with increasing $\mathcal{E}_0$ is present), and the extended states with $\sigma_n \approx 32$ exist at moderate and strong driving, meaning the presence of diffusion in the Hilbert space into a substantial part of the spectrum totaling 108 levels for the chosen set of model parameters. We can see from Fig. 2*b* that the difference between the quasienergy state statistics for $\mathcal{E}_0 = 1$ V/cm and $\mathcal{E}_0 = 2$ V/cm is only quantitative, because both fields correspond to the quasiclassically unstable regions, and therefore only moderate driving fields not exceeding the scale of 1 V/cm are required for the excitation of irregular or chaotic regimes in our system.

We thus conclude that the analysis of Floquet eigenstates demonstrates the possibility of excitation of diffusion regimes in the Hilbert space if the initial states are located in the region of the maximum variance $\sigma_n$ near the center of the spectrum. In the next section, we confirm this assumption by integrating the nonstationary Schrödinger equation with the Hamiltonian

$H_{qd} + V(y, t)$ over a continuous time interval. The reason for such an approach is that a substantial part of the evolution occurs between the stroboscopic moments of time $T_n = nT_0$, which are in the focus of the Floquet stroboscopic approach. To obtain a more detailed picture, we proceed with direct numerical integration for continuous time with a suitable time grid catching all the essential details of the dynamics, and also providing a perfect match between the continuous and Floquet approaches.

## 5. EVOLUTION IN THE CLEAN LIMIT

We begin with the analysis of the driven evolution of the wide wavepacket (see Fig. 1*c,d*), which is described by Schrödinger equation (27) with the moderate amplitude $\mathcal{E}_0 = 1$ V/cm of driving electric field (10). The initial state $C_n(0)$ occupies a narrow part of the Hilbert space near the center of the spectrum, as can be seen in Fig. 1*d*. We solve the equations of motion for $C_n(t)$ from several hundred to several thousand periods $T_0 = 2\pi/\omega_0$, which is the unit of time in our model, where $\hbar\omega_0$ is the spacing between a selected pair of levels near the center of the spectrum.

The initial state of the wavepacket injected from the left barrier into the QD is characterized by the spin polarization in units of $\hbar/2$ as $S_x = 1$, $S_y = S_z = 0$. As we have mentioned in Sec. 2, for all basis states (4)–(6) the mean spin is always in the plane of the 2D TI, that is, $S_z = 0$. However, if a time-dependent mixture (26) of such states is formed by the initial packet or by the nonstationary driving $V(y, t)$, the resulting spinor wavefunction may correspond to the state where the out-of-plane $S_z$ spin component is present. We discuss this in detail below.

We look at the evolution of the quantum mechanical mean values, or observables, for several variables of interest, for both coordinate and spin degrees of freedom. As is known from classical mechanics, the evolution of a driven system can be represented in terms of canonically conjugate variables such as $(x_i, dx_i/dt)$ shown in phase plots. For a quantum mechanical system, the concept of trajectories is not directly available, and the dynamics of mean values of such variables can be considered. The velocity operator introduced as $dx_i/dt = (i/\hbar)[H, x_i]$ gives the following form for $v_y = dy/dt$ and Hamiltonian (2):

$$v_y = v_F \sigma_z. \qquad (29)$$

We note that the time dependence of the mean value in Eq. (12a) is obtained for the quasiclassical dynamics.

This result means that the velocity is effectively represented on the "phase-space plot" by the $z$ component of spin, and hence the first pair of the mean values to be plotted is $(y, S_z)$. For brevity in what follows, we omit the $\overline{(\dots)}$ mark for mean values plotted on Figures. For our model of coordinate and spin dynamics, this means that these two channels are tightly coupled from the very beginning, and we can expect certain common characteristics of their evolution, as was already shown for a semiconductor mesoscopic QD with spin–orbit coupling [21].

The general expressions that allow us to calculate the mean values of coordinate and velocity for state (26) via the matrix elements $y_{ij}$ of the position operator $y$ are

$$\overline{y}(t) = \sum_{ij} C_i^*(t) C_j(t) y_{ij}, \qquad (30)$$

$$\overline{v_y}(t) = \frac{i}{\hbar} \sum_{ij} C_i^*(t) C_j(t) (E_i - E_j) y_{ij}. \qquad (31)$$

We can see that the velocity mean value (31) is directly related not only to the spin via (29) but equivalently to the position operator $y$ because its matrix elements define both expressions (30) and (31) together with the energy level structure. By comparing two approaches (29) and (31) for the velocity operator, we can see that in the present model, the spin projection indeed plays the role of momentum for a classical spinless oscillator with finite mass. Hence, we can expect the phase plots for the coupled coordinate and spin dynamics to bear some resemblance to the conventional phase plots for the driven oscillator plotted for the $(y, v_y)$ variables. It can be mentioned that for a strictly equidistant spectrum $E_i - E_j = \hbar\omega_0$ it follows from (30) and (31) that $\overline{v_y} = i\omega_0\overline{y}$ just as for the linear oscillator. In our model, however, the level spacing is not purely constant, and such a simple relation is only approximate but not exact.

The second pair of variables to be plotted together is the in-plane spin projection represented by the mean values of $(S_x, S_y)$ spin components. This choice is motivated by the inherent structure of Hamiltonian (2). Namely, the internal part of the QD region is described by the Weyl Hamiltonian coupling the $(y, S_z)$ degrees of freedom, and the surrounding barriers are polarized in the $(S_x, S_y)$ plane, which also couples these two spin components to other degrees of freedom. As a result, the spin vector is subject to evolution for all its projections that are coupled to the one-dimensional spatial motion along the $y$-direction in the QD. Such pairs of spin variables have been considered in several studies on spin-resolved systems [16, 21, 23], and are convenient,

for example, in representing the in-plane spin precession.

For numerical calculations, we consider the time interval of 400 periods of the driving field with 200 points per period for the graphical representation. These parameters cover both the time span needed for the stationary regime of the dynamics to be established and the time grid that catches the significant nonvanishing Fourier components of the evolution of observables.

In Fig. 3, we show the results for the driven evolution for the initial state represented by the wide wavepacket from Fig. 1$c$ with the zero mean value of the quasimomentum, $\overline{k_y}(0) = 0$. The initial point at $t = 0$ is marked as the black circle A. Panel $a$ shows the "phase space" plot of the evolution in the $(y, S_z)$ coordinates and panel $b$ shows the in-plane spin precession in the $(S_x, S_y)$ plane. In Fig. 3$c$, the evolution of the variance of the level number $\sigma_n(t)$ is shown, which describes the spreading of the initial state $C_n(0)$ in the Hilbert space of the basis states. Also, we are interested in the dynamics of the variance $\sigma_y(t)$ for the packet width in the coordinate space,

$$\sigma_y^2(t) = \overline{(y - \overline{y}(t))^2}. \qquad (32)$$

The time dependence for this quantity is shown in Fig. 3$d$. It is also of interest to look at the spatial distributions along the QD for the charge density $\rho(y, t_0)$ and some of the spin density components $S_i(y, t_0)$, $i = x, y, z$, at certain moments of time. The spatial profiles of charge and spin density are helpful in understanding on which spatial scale the charge and spin spots can be measured in actual experimental setups. We present an example of charge and spin densities plotted at a specific moment of time in Fig. 3$e$.

Besides tracking the evolution of the mean values, we are interested in their Fourier power spectra

$$I_\xi(\omega) = \left| \int_{-\infty}^{\infty} \xi(t) e^{-i\omega t} dt \right|^2, \qquad (33)$$
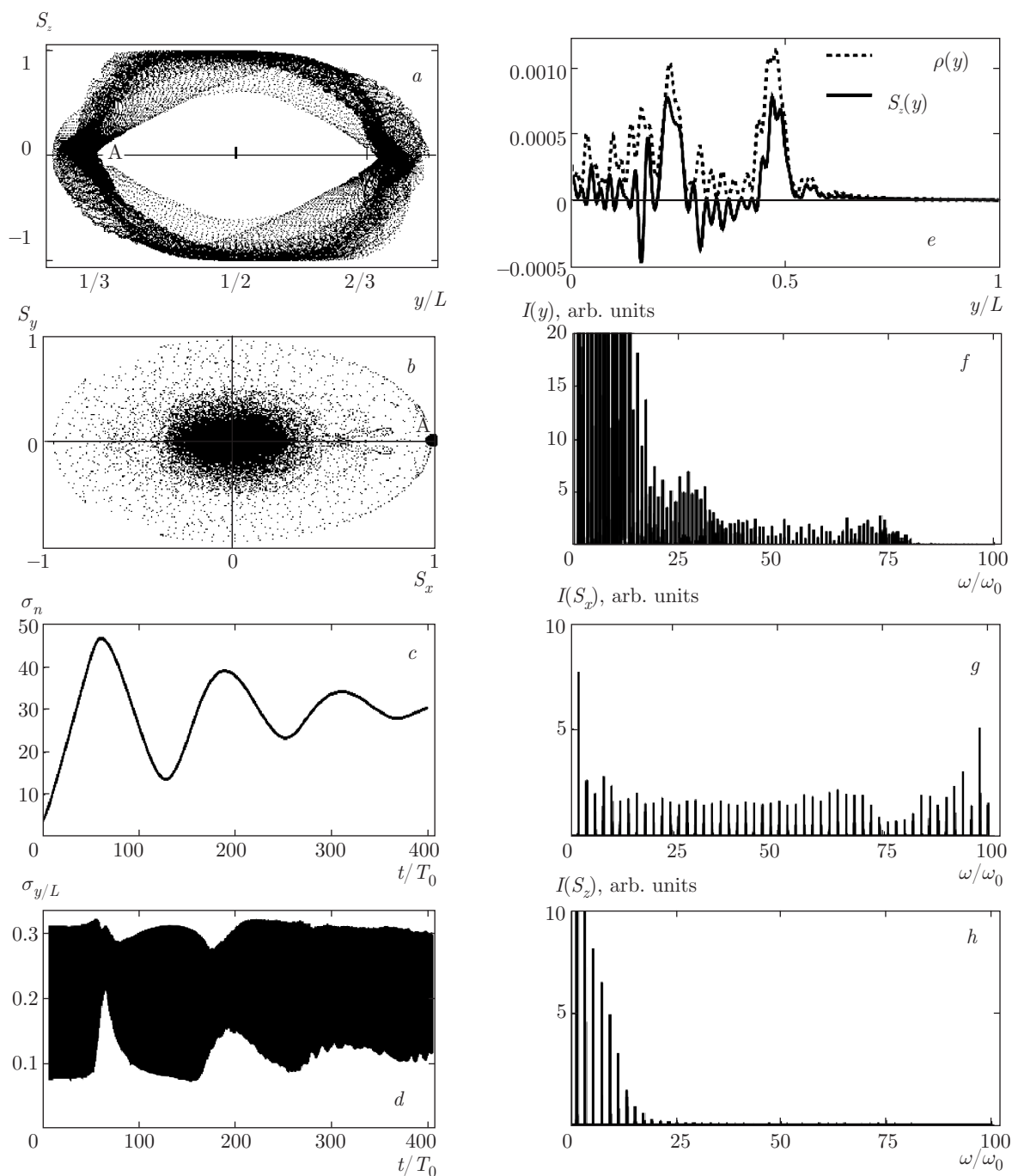
where $\xi$ is the variable of interest. Because we obviously consider large, but finite intervals of time, Fourier power spectra (33) are calculated by the fast Fourier transform with limits of time actually used in our simulations of the dynamics. In panels $f$, $g$, and $h$ in Fig. 3, we show the Fourier power spectra for the variables $y$, $S_x$ and $S_z$.

We now discuss the meaning of the results presented in Fig. 3. First, we consider the trajectories in the space of $(y, S_z)$ and $(S_x, S_y)$ pairs of variables shown in Fig. 3$a,b$. We can see that the regular trajectories for

these phase plots are accompanied by the surrounding areas of a "chaotic sea", although the general oscillating character of the wavepacket evolution is still visible. We can say that the phase portrait in Fig. 3$a$ in general resembles the phase trajectories of a driven classical oscillator in the irregular regime of dynamics. The onset of irregular motion is further pronounced in the in-plane spin dynamics in Fig. 3$b$. In general terms, we can state that the spin evolution becomes largely irregular. As was found in Sec. 3, the quasiclassical spin dynamics for the driving field amplitude $\mathcal{E}_0 = 1$ V/cm corresponds to the unstable region of Mathieu equation (23). We see that the full quantum mechanical treatment leads to the same conclusion about the onset of chaotic dynamics for the electric field amplitude and frequency corresponding to a quasiclassically unstable area. Another justification for the correspondence between the full quantum mechanical and quasiclassical treatment is the initial wavepacket width considered here. In this section, it corresponds to a narrow distribution in the Hilbert space of the basis states, which makes the quasiclassical approach applicable, and the main conclusions from the quasiclassical and full quantum approaches support each other.

As regards the spin dynamics in general, we can describe it as a combination of precessions with generally incommensurable frequencies around the directions of effective magnetic fields following from Hamiltonian (2): the $z$-oriented $k_y$-dependent field inside the QD and the $x$-oriented barrier field. As a result, the spin dynamics becomes rather complex. A large clustering area near the origin for the in-plane components $(S_x, S_y)$ reflects the larger frequency of precession around the $z$-aligned effective magnetic field inside the QD, where the wavefunction is mostly located, resulting in the averaged in-plane spin components $(S_x, S_y)$ being close to zero, as we can see in Fig. 3$b$. The observed spin precession can be regarded as being typical for systems with strong spin–orbit coupling, which was found, for example, for the models of spin dynamics in semiconductor QDs [16, 17].

The concept of irregular dynamics or chaos development can be supported by the analysis of the driven evolution in the Hilbert space of basis states. Here, the onset of chaos usually corresponds to the growth in time of the number of energy levels involved in the evolution, which is sometimes called the quantum Arnol'd diffusion [13]. Our Floquet analysis of the quasienergy eigenfunctions in Sec. 4 indicates that the periodic driving with amplitudes in the range 1–2 V/cm can induce the formation of Floquet states that are deeply extended into a substantial part of the energy spec-

**Fig. 3.** (*a*) Evolution in the "phase space" of the mean values $(y, S_z)$ for the amplitude $\mathcal{E}_0 = 1$ V/cm of the driving electric field. (*b*) Evolution of the in-plane spin components $(S_x, S_y)$. The initial point at $t = 0$ is shown as the black circle A. The in-plane spin components demonstrate the tendency to clustering near the zero values with growing time. (*c*) The evolution in the Hilbert space plotted as the number of levels effectively participating in the dynamics shows a linear growth at the beginning of the evolution, which corresponds to the chaotic regime. (*d*) The packet half-width variance describing the spreading of the wavepacket in the real space inside the QD. The initial half-width (see Fig. 1*c*, packet (1)) does not grow with time, and, as for the free evolution, the packet is narrowed at certain moments of time. (*e*) Charge density $\rho(y)$ (dashed curve) and the $S_z(y)$ component of spin density (solid curve) inside the QD taken at $t = 395T_0$. (*f*),(*g*),(*h*) Fourier power spectra (31) for the $y$, $S_x$, and $S_z$

trum (see Fig. 2). Thus, we can expect the variance $\sigma_n$ measuring the number of levels involved in the evolution to be as high as the maximum number reached by the Floquet states. This assumption is confirmed by the plot of $\sigma_n(t)$ in Fig. 3c, where an almost linear increase in the level number is present at the initial stage of evolution, where the quantum–classical correspondence is most pronounced [9–11]. Such an increase is usually attributed to the onset of chaotic dynamics, or diffusion in the Hilbert space, which provides another correspondence between the findings on the instability regions within the quasiclassical approach in Sec. 3 and the full quantum mechanical treatment. After some time, however, the discrete character of the quantum mechanical spectrum of a finite motion inside the QD leads to a saturation of the level number involved in the evolution, and the diffusion in the Hilbert space effectively stops [13]. This can be seen in Fig. 3c, where the linear growth of $\sigma_n$ yields to oscillations with a stable mean value. We can say that the chaotic behavior has a transient nature in our quantum system.

As regards the dynamics in real space inside the QD, the evolution of the packet half-width is presented in Fig. 3d. The packet width essentially does not grow with time, and the packet at each moment of time effectively occupies only a limited area inside the QD. This finding is illustrated by the example of the spin and charge density distributions inside the QD shown for $t = 395T_0$ in Fig. 3e. We can see that the packet occupies a substantial part of the QD, but its effective width has a value close to the width of the initial packet (Fig. 1c, wavepacket (1)). As we have mentioned, such stable behavior of the packet width during the driven evolution can be attributed to the nearly equidistant character of the energy levels of the system, which can trigger certain properties of coherent states in the driven evolution.

The manifestation of chaotic or at least strongly irregular regimes for the driven evolution is supported by the Fourier power spectra for the coordinate and spin observables plotted in Fig. 3f–h. We can see that the driving induces a large number of harmonics of the driving frequency $\omega_0$ for both the coordinate and spin, especially the in-plane component $S_x$ (and similarly for $S_y$, which is not shown here). The presence of a large number of harmonics is a strong indication of irregular dynamics [9, 16, 21], which supports the quasiclassical results in Sec. 3 on the onset of unstable dynamics for the considered amplitude of the driving field.

Another possible manifestation of chaos is the presence of positive Lyapunov exponents [9, 10] that measure the rate of divergence of two initially close trajec-
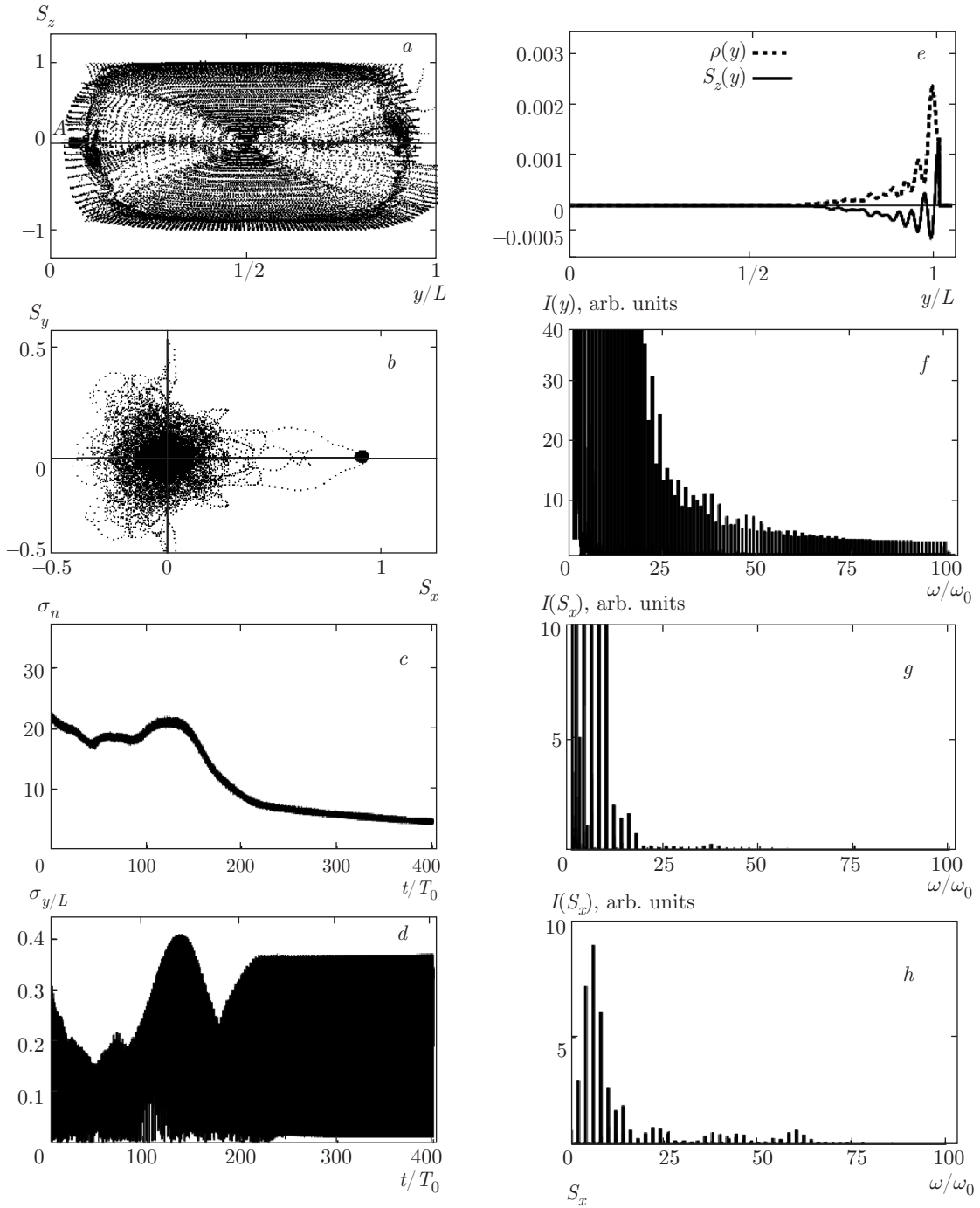
tories in the phase space,

$$\lambda = \lim_{t \to \infty} \frac{1}{t} \log \frac{d(t)}{d(0)}, \tag{34}$$

where $d(t)$ and $d(0)$ are the current and initial distances. The infinite limit in (34) can also be tracked by continuously monitoring with the growing time, where $\lambda = \lambda(t)$ tracks a local transition between the regular and chaotic regimes. In Fig. 5 below, we plot the dependence of $\lambda(t)$ for two initially close wavepackets whose mean values of the coordinate are shifted slightly along $y$ at $t = 0$. We can see that at the beginning of the evolution, the region with positive $\lambda(t)$ indeed exists, which corresponds to the linear growth of the level number $\sigma_n$ involved in the dynamics (see Fig. 3c). Both these plots support the presence of the chaotic dynamics at the initial stage of the evolution when the discrete character of the quantum spectrum has not yet manifested itself so much. After the initial transient period, the evolution tends to transform to a quasiregular regime with a stable number of levels involved in the dynamics, and the Lyapunov exponent reduces to zero, as can be seen in Fig. 5 below. We note that such a behavior is known in quantum systems with irregular dynamics [9–11, 13]. However, the results obtained there mainly pertain to spinless systems with a quadratic spectrum having a certain classical analogue.

To conclude this section, we can state that even in a quantum system that lacks a classical analogue such as the system with Hamiltonian (2), we can observe certain traits of the development of irregular phenomena that are present in classically chaotic systems and are in good agreement with the quasiclassical treatment. We stress that such effects may arise in the considered structures at driving fields as low as several V/cm. This means that apart from the fundamental questions on the degree of irregularity of the electron and spin dynamics in systems with strong spin–orbit coupling, our findings can also be important for nanodevice designers and experimenters for future applications of the TI-based structures.

## 6. EVOLUTION IN THE PRESENCE OF DISORDER

The presence of some kind of disorder in the form of a spatially nonuniform potential at the TI edge or the potential caused by defects is inevitable in any real structure and should be addressed in the problem of

**Fig. 4.** The same as in Fig. 3 but for a narrow wavepacket (see Fig. 1c,e) taken as the initial condition, and in the presence of disorder potential (35) with the amplitude $U_0 = 0.5$ meV. (a),(b) Phase plots for the coordinate and spin mean values shown for pairs $(y, S_z)$ and $(S_x, S_y)$, respectively. The in-plane spin components show an enhanced tendency to clustering near the zero values with growing time. (c) Evolution in the Hilbert space of $\sigma_n$ demonstrates the decreasing number of basis states participating in the evolution, which can be viewed as an example of localization in the Hilbert space. (d) The packet half-width dynamics shows the amplitude stability on long times. (e) An example of the charge and spin density for $t = 395 T_0$ demonstrates a well-localized packet even in the presence of a strong disorder potential. (f),(g),(h) Fourier power spectra for the coordinate $y$ and two spin components $S_x$ and $S_z$ showing the behavior where disorder can enhance the in-plane spin relaxation

the electron evolution. In this section, we insert an additional stationary disorder potential of the form
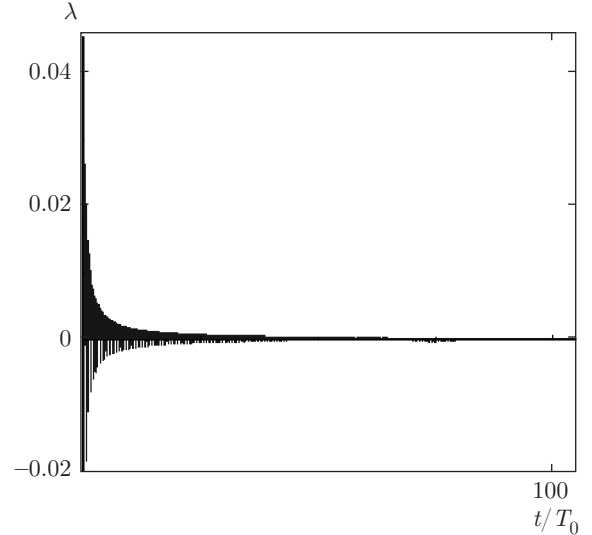
$$U_d(y) = U_0 f(y) \qquad (35)$$

into the right-hand side of non-stationary Schrödinger equation (27), where the potential amplitude $U_0$ is multiplied by a random function $f(y)$ described by a uniform random distribution from 0 to 1 along the QD, with $0 \leq y \leq L$. It is known that the presence of disorder alone with the potential that maintains the time-reversal invariance such as the scalar potential in (35) does not break the topological protection of the edge states. For the QD considered in our model, time reversal symmetry has already been broken by the presence of magnetic barriers, and hence the disorder potential, for example, may induce transitions between states with different spin polarizations.

The interest in the influence of an external disorder potential on the wavepacket evolution in materials such as Dirac-fermion materials started to arise during the last years, sometimes leading to unexpected results. For example, it was shown recently that the inclusion of a static 1D disorder potential into the model of wavepacket propagation in graphene and related Dirac-fermion materials may cause the so-called electron supercollimation, i.e., the effect when the wavepacket moves undistorted along a certain direction [30]. It is therefore a challenging and intriguing task to consider the effects of the disorder potential on the driven dynamics in our model of the QD in a TI.

The matrix elements of $U_d(y)$ in (35) contribute to the dynamics of the coefficients $C_n(t)$ for wavefunction (26) together with the ones from the driving term $V(y,t)$. We consider the example of the amplitude $U_0 = 0.5$ meV, which is comparable with typical interlevel distance (8) equal to 0.38 meV (i.e., we insert a moderate disorder). This can be justified by a typical high quality and high mobility of samples usually fabricated and studied in the experiments with TIs [7], which have the mean free path of the order of the QD length $L$, and low temperatures around or below 1 K, which produces the level broadening of the order of 0.05 meV. For the initial condition, we choose a narrow wavepacket (see the packet profile shown by curve 2 in Fig. 1c). We take the same driving amplitude $\mathcal{E}_0 = 1$ V/cm, and the same other parameters as in the preceding section.

We can expect certain modifications of the evolution for both coordinate and spin degrees of freedom when the disorder amplitude $U_0$ exceeds the energy of the driving field. In Fig. 4, we show the evolution of a narrow wavepacket under the driving with $\mathcal{E}_0 = 1$ V/cm,



**Fig. 5.** Evolution of Lyapunov exponent (34) for two initially close wavepackets. At the beginning of the evolution, this exponent also takes positive values, indicating the presence of a chaotic regime, and later it decreases to zero when the quasi-regular quantum dynamics is established

with the disorder amplitude $U_0 = 0.5$ meV that exceeds the typical energy of the driving field $e\mathcal{E}_0 L = 0.3$ meV. The numbering of the figure panels is similar to that in Fig. 3. We can see that the inclusion of disorder leads to more uniformly distributed trajectories in the phase space of the $(y, S_z)$ variables shown in Fig. 4a. We can say that disorder reduces the degree of correspondence with phase plots for the classical driven oscillator. The in-plane spin components $(S_x, S_y)$ demonstrate a more pronounced tendency to cluster near the coordinate origin $(0,0)$ with growing time, meaning that the spin precession here is accompanied by collisions of an electron with the inhomogeneities of potential (35) and leading to the effective spin relaxation. As regards the off-plane spin component $S_z$, it still demonstrates a full-scale oscillating behavior representing the electron velocity in our model, but within a well-established chaotic sea visible in the $(y, S_z)$ plot. The disorder leads to an interesting effect on the number of levels $\sigma_n$ effectively involved in the evolution, which is shown in Fig. 4c. Starting from the initially large number of basis states present in the decomposition of a narrow wavepacket, this number begins to decrease progressively, with the average level number (not shown) moving down from the Dirac point. Such a form of localization in the Hilbert space can be viewed as a decrease in the irregularity when the dynamics of the system in fact becomes more regular in terms of the number of states involved in the evolution. We can say that the presence of static

disorder inhibits the development of dynamical chaos, although it does not suppress it completely.

The variance of the packet half-width given in Fig. 4*d* shows the oscillating behavior with a saturating amplitude, which again demonstrates the effect of the wavepacket maximum width stability induced by the periodic driving, which is maintained even in the presence of strong disorder. An example of the charge $\rho(y)$ and spin density $S_z(y)$ distributions at the end of the observation frame $t = 395T_0$ shown in Fig. 4*e* supports this finding, demonstrating a well-localized packet near one of the edges of the QD. These findings regarding the dynamics are supported by the Fourier power spectra shown in Fig. 4*f–h*, where the spin components demonstrate a more rapidly vanishing spectra compared to the coordinate one. This can be attributed to the effects of spin precession in the presence of collisions caused by disorder. We can say that the observed effects of disorder to some extent lead to a reduction in the dynamical chaos. This observation is important for further experimental and technological applications because the presence of some degree of disorder is inevitable in real structures, and in certain cases it can play a positive role as a damper of chaotic regimes of the dynamics.

To conclude this section, we can say that by comparing Fig. 3 and Fig. 4, we see that the principal features of almost all respective panels on these figures look similar. In contrast, the initial wavepacket in Fig. 3 is described by the quasiclassically tractable narrow distribution in the Hilbert space of basis states, while the initial wavepacket in Fig. 4 is described by a wide distribution for which the full quantum simulation is required. This similarity can be viewed as an additional argument supporting the applicability of the quasiclassical approach derived in Sec. 3, because the full quantum treatment leads to the principally close results for both regions with or without the possibility to apply the quasiclassical method.

## 7. CONCLUSIONS

We have studied the dynamics of Dirac–Weyl wavepackets driven by a periodic electric field in a mesoscopic QD formed at the edge of the two-dimensional HgTe/CdTe topological insulator, where the motion of carriers is less sensitive to disorder and impurity potentials. It was found that the presence of strongly coupled spin and charge degrees of freedom in such a driven system leads to the regimes of transiently irregular dynamics both in the clean limit and in the presence of the disorder. The quasiclassical analysis of

spin dynamics allowed analytically finding the border between the regular and irregular regimes defined by the amplitude and frequency of the driving field in the framework of the Mathieu equation, and was supported by the full quantum mechanical treatment. The predicted onset of irregular regimes in both coordinate and spin channels, which occurs for a mesoscopic QD at the amplitudes of driving fields being as low as $1 \ldots 2$ V/cm is, in our opinion, an important feature of the considered structures from both fundamental and device-oriented standpoints. The observed effects of disorder can be described in general as damping of the chaotic regimes of dynamics, which is also important for possible experiments in real structures. We believe that our findings are not limited to 1D edges of 2D topological insulators based on HgTe/CdTe quantum wells but also apply to other systems with a Dirac–Weyl spectrum, which allows considering them as being rather general. Apart from the basic questions on the degree of irregularity of the electron and spin dynamics in systems with strong spin–orbit coupling, our findings can also be taken into consideration by nanodevice designers and experimenters who plan to use the topological-insulator-based structures for transport and information processing purposes, where the manifestations of irregularity even at low driving fields may seriously affect their operational capabilities.

## REFERENCES

1. G. E. Volovik, *The Universe in a Helium Droplet*, Clarendon Press, Oxford (2003).

2. P. B. Pal, Amer. J. Phys. **79**, 485 (2011).

3. Z. Lan, N. Goldman, A. Bermudez et al., Phys. Rev. B **84**, 165115 (2011).

4. O. Vafek and A. Vishwanath, Ann. Rev. Cond. Matt. Phys. **5**, 83 (2014).

5. X. Wan, A. M. Turner, A. Vishwanath et al., Phys. Rev. B **83**, 205101 (2011).

6. C. W. Beenakker, Rev. Mod. Phys. **80**, 1337 (2008).

7. B. A. Bernevig, *Topological Insulators and Topological Superconductors*, Princeton University Press, Princeton (2013); S. Q. Shen, *Topological insulators. Dirac equation in Condensed Matter*, Springer Series in Solid-State Science, Springer-Verlag, Berlin, Heidelberg (2012); M. Z. Hasan and C. L. Kane, Rev. Mod. Phys **82**, 3045 (2010); X.-L. Qi and S.-C. Zhang, Rev. Mod. Phys. **83**, 1057 (2011).

8. V. A. Volkov and I. V. Zagorodnev, Low Temper. Phys. **35**, 2 (2009).

9. M. C. Gutzwiller, *Chaos in Classical and Quantum Mechanics*, Springer-Verlag, New York (1990).

10. L. E. Reichl, *The Transition to Chaos. Conservative Classical Systems and Quantum Manifestations*, 2nd Ed., Springer-Verlag, New York (2004).

11. H.-J. Stöckmann, *Quantum Chaos: An Introduction*, Cambridge University Press (1999).

12. K. Nakamura and T. Harayama, *Quantum Chaos and Quantum Dots*, Oxford University Press, New York (2004).

13. V. Ya. Demikhovskii, F. M. Izrailev, and A. I. Malyshev, Phys. Rev. Lett. **88**, 154101 (2002); Phys. Rev. E **66**, 036211 (2002); A. I. Malyshev and L. A. Chizhova, J. Exp. Theor. Phys. **110**, 837 (2010).

14. I. Žutić, J. Fabian, and S. Das Sarma, Rev. Mod. Phys. **76**, 323 (2004).

15. *Spin Physics in Semiconductors*, ed. by M. I. Dyakonov, Springer-Verlag, Berlin, Heidelberg (2008).

16. D. V. Khomitsky and E. Ya. Sherman, Phys. Rev. B **79**, 245321 (2009).

17. D. V. Khomitsky, L. V. Gulyaev, and E. Ya. Sherman, Phys. Rev. B **85**, 125312 (2012).

18. L. Chotorlishvili, Z. Toklikishvili, A. Komnik et al., Phys. Lett. A **377**, 69 (2012); J. Phys.: Condens. Matt. **24**, 255302 (2012).

19. K.-F. Berggren and T. Ouchterlony, Found. Phys. **31**, 233 (2001).

20. O. V. Marchukov, A. G. Volosniev, D. F. Fedorov et al., J. Phys. B: At. Mol. Opt. Phys. **47**, 195303 (2014).

21. D. V. Khomitsky, A. I. Malyshev, E. Ya. Sherman et al., Phys. Rev. B **88**, 195407 (2013).

22. K.-F. Berggren, A. F. Sadreev, and A. A. Starikov, Phys. Rev. E **66**, 016218 (2002); E. N. Bulgakov, D. N. Maksimov, and A. F. Sadreev, Phys. Rev. E **71**, 046205 (2005); E. N. Bulgakov and I. Rotter, Phys. Rev. E **73**, 066222 (2006); K.-F. Berggren, D. N. Maksimov, A. F. Sadreev et al., Phys. Rev. E **77**, 066209 (2008).

23. Z. Yang, S. Zhang, and Y. C. Li, Phys. Rev. Lett. **99**, 134101 (2007).

24. B. A. Bernevig, T. L. Hughes, and S.-C. Zhang, Science **314**, 1757 (2006); M. König, H. Buhmann, L. W. Molenkamp et al., J. Phys. Soc. Jpn. **77**, 031007 (2008).

25. C. Timm, Phys. Rev. B **86**, 155456 (2012).

26. A. Kundu, A. Zazunov, A. L. Yeyati et al., Phys. Rev. B **83**, 125429 (2011); G. Dolcetto, N. Traverso Ziani, M. Biggio et al., Phys. Rev. B **87**, 235423 (2013); G. J. Ferreira and D. Loss, Phys. Rev. Lett. **111**, 106802 (2013); C. Ertler, M. Raith, and J. Fabian, Phys. Rev. B **89**, 075432 (2014).

27. G. Giavaras, P. A. Maksym, and M. Roy, J. Phys. Cond. Mat. **21**, 102201 (2009); G. Giavaras and F. Nori, Phys. Rev. B 83, 165427 (2011); Phys. Rev. B **85**, 165446 (2012).

28. *Handbook of Spin Transport and Magnetism*, ed. by E. Y. Tsymbal and I. Žutic, CRC Press, Taylor and Francis Group, Boca Raton (2012); *Nanoscale Magnetic Materials and Applications*, ed. by J. P. Liu, E. Fullerton, O. Gutfleisch, and D. J. Sellmyer, Springer Science+Business Media, New York (2009); *Magnetism. Materials and Applications*, ed. by É. du Trémolet de Lacheisserie, D. Gignoux, M. Schlenker, Springer Science+Business Media, Boston (2005).

29. D. R. Merkin, *Introduction to the Theory of Stability*, Springer-Verlag, New York, Inc. (1997).

30. S. Choi, C.-H. Park, and S. G. Louie, Phys. Rev. Lett. **113**, 026802 (2014).